Proceedings of the 5th International Conference on Nanochannels, Microchannels & Minichannels
ICNMM2007
June 18-20, 2007, Universidad De Las Americas Puebla, Mexico

ICNMM2007-30135

NUMERICAL ANALYSIS OF THE 3D FLOW INDUCED BY PROPAGATION OF PLANE-WAVE DEFORMATIONS ON THIN MEMBRANES INSIDE MICROCHANNELS

Ahmet Fatih Tabak[*,1] **Serhat Yeşilyurt**[*,2]
[*]**Sabanci University, Istanbul, Turkey**
[1]**tabak@su.sabanciuniv.edu,** [2]**syesilyurt@sabanciuniv.edu**

ABSTRACT

Propulsion mechanisms of microorganisms are based on either beating or screw-like motion of thin elastic biopolymers. Arguably, this motion is optimal for propulsion at very low Reynolds numbers. Similar actuation mechanisms can be utilized in the design of an autonomous microswimmer or even a micropump. In principle, propagation of plane-wave deformations on a thin-membrane placed inside a channel can lead to a net flow in the direction of the wave propagation. In this study we present effects of the amplitude, frequency, and the width of the membrane on the time-averaged flow rate and the rate of work done on the fluid by the membrane by means of three-dimensional transient simulations of flows induced by plane-wave deformations on membranes. Navier-Stokes and continuity equations are used to model the flow on a time-varying domain, which is prescribed with respect to the motion of the membrane. Third party commercial software, COMSOL, is used in to solve the finite-element representation of the 3D time-dependent flow on moving mesh. Numerical simulations show that the flow inside the microchannel depend on the square of the amplitude and is proportional to the excitation frequency. Lastly, characteristic flow rate vs. pressure head curve and efficiency of a typical pump are obtained from 3D transient simulations, and presented here.

INTRODUCTION

Time reversible reciprocating actuation mechanisms can not sustain significant net flow under low Reynolds Numbers where shear forces are dominant over inertial forces as explained in 'scallop theorem' [1]. Microorganisms such as spermatozoa and bacteria use their flagella to propel themselves [2]. Flagella of spermatozoa and other eukaryotic cells resemble to elastic rods, whose stress-induced sudden-bending deformations propagate in waves towards the tip in a way similar to beating motion [3]. Periodic traveling-wave deformations of the biopolymer tail of the microorganism are the result of the balance between the bending stresses of the structure and the total stress in the fluid [4].

Propulsion mechanisms of microorganisms can be a viable option in producing controllable flows for micropump applications [5] as well as propulsion of autonomous micro swimming robots [6]. Continuous traveling sinusoidal waves on fully submerged thin membranes constitute as a time-irreversible actuation mechanism. It was shown that net propulsion can be obtained by magnetic filaments attached to blood-cells driven by external magnetic fields [7]. Moreover, three-dimensional numerical investigation of surface acoustic waves created by inter-digital transducers on a thin membrane exhibits the dependence of the fluid flow on the wave amplitude and the actuation frequency in microfluidic applications [8].

Vertical motion of the fully submerged elastic membrane causes dynamic high and low pressure regions resulting in a flow between them. As the deformation shifts position accordingly with the propagation of traveling waves, high and low pressure regions in the vicinity of the membrane demonstrate consequential shifts which result in a net flow in propagation direction. This relation between pressure and deformation was deduced by means of work exerted on the fluid by the deforming membrane [9].

Despite their limited deformation amplitude, thin piezoelectric sheets can be used to form plane-wave deformations [10,11]. Structural analysis of the thin-membrane and its optimization are already discussed

elsewhere [12] partially, and beyond the scope of this work.

Sir Taylor presented asymptotic solutions of the flow for a sinusoidal wave propagating on an infinite inextensible sheet immersed in viscous fluid [13]. Later, Katz presented an asymptotic solution for the infinite sheet placed inside a channel [14]. Our previous work verifies asymptotic results of Taylor [13] and Katz [14] by means of numerical solution of the two-dimensional time-dependent Stokes flow due to plane waves traveling on a finite-length thin membrane inside a channel [15].

In this work, we present numerical solutions of 3D time-dependent channel flows induced by the propagation of sine-wave deformations on thin-membranes submersed in fluids inside channels. These flows are governed by incompressible Navier-Stokes equations subject to continuity on time-varying domains. Mesh displacement due to moving boundaries of the membrane is modeled using an arbitrary Lagrangian-Eulerian formulation [16]. Effects of the amplitude, frequency and the film's width are demonstrated. Pressure head and efficiency against the flow rate curves are shown for a typical micropump that is actuated by traveling-sine-wave deformations on a thin-membrane.

NOMENCLATURE

Symbol	Description
Latin Letters	
A	Area
B_o	Maximum wave amplitude
H	Channel height
I	Identity matrix
L	Channel length
P	Liquid pressure
Q	Flow rate
U	Fluid velocity vector
W	Width
dy	Mesh deformation in Ω
f	Excitation frequency [Hz]
k	Wave number
ℓ_f	Membrane length
n	Surface normal vector
t	Spatial time
u	Mesh velocity vector
u,v,w	velocity components
x,y,z	Spatial coordinates
Functions and Groups	
B	Amplitude expression
min	Minimum function
Re	Reynolds Number
Greek Letters	
Π	Mechanical Power exerted on fluid
Σ	Mono directional full stress tensor
Ω	Domain occupied by fluid inside
η	Percentage mechanical efficiency
λ	Wave length
μ	Dynamic viscosity of liquid
ρ	Liquid density
ω	Angular frequency
Subscripts and Superscripts	
$A.av$	Area-averaged
av	Time-averaged
ch	Channel parameter
f	Membrane parameter
in,out	Inwards/outwards direction
m	Mesh parameter
T	Transpose
0	Characteristic scale

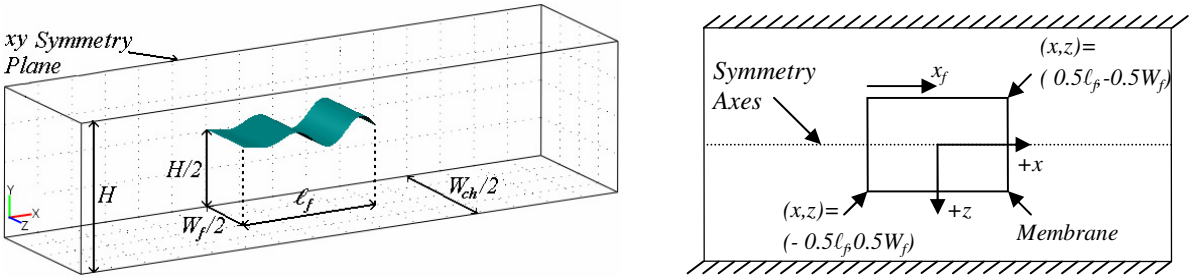

(a) (b)

Figure 1: (a) Plane-wave deformations traveling in the z-direction on the thin membrane placed in a channel; (b) Top-view in the y-direction on the x-z plane.

METHODOLOGY

Motion of the thin-membrane is limited to the y-axis, which is perpendicular to the wave propagation in the x-direction as shown in Fig. 1. Y-axis motion of the membrane, which is due to traveling-wave deformations, is given by a sinusoidal wave-form as a function of time, t, x-position on the membrane, x_f, excitation frequency, $\omega=2\pi f$, wave number, $k=2\pi/\lambda$ and the amplitude B, i.e. we have

$$y_f\left(x_f,t\right)=B\sin\left(\omega t-kx_f\right) \qquad (1)$$

In Eq. (1), $B=B(x,t)$ defines an envelope for the extent of the deformations in the y-direction and keeps one end of the membrane. Furthermore, to ensure zero initial conditions, an initial ramp of the amplitude of deformations is defined and restricted to the first full period:

$$B\left(x_f,t\right)=B_o\tanh(x_f)\min\left(t,\frac{1}{f}\right) \tag{2}$$

Although Stokes equation suffices to describe the flow, to allow local inertial effects incompressible Navier-Stokes equations are used to model the three-dimensional time-dependent flow in the time-dependent domain $\Omega(t)$ subject to the continuity equation:

$$\rho\left(\frac{\partial\mathbf{U}}{\partial t}+\left(\mathbf{U}-\mathbf{u}_m\right)\cdot\nabla\mathbf{U}\right)=-\nabla P+\mu\nabla^2\mathbf{U} \tag{3}$$

$$\nabla\cdot\mathbf{U}=0 \tag{4}$$

where $\mathbf{U}=[u,v,w]^{\mathrm{T}}$ is the velocity vector, P is pressure, ρ is density, and μ is the viscosity of the fluid. The time-dependent deforming domain, $\Omega(t)$, is the volume occupied by the fluid inside the channel. The $\mathbf{u}_m$ in Eq. (3) is the deformation velocity of the domain $\Omega(t)$ [16], which is induced due to moving boundaries of the membrane.

Channel walls are subjected to no-slip boundary conditions,

$$\begin{bmatrix}u(x,0,z,t)\\v(x,0,z,t)\\w(x,0,z,t)\end{bmatrix}=\begin{bmatrix}u(x,H,z,t)\\v(x,H,z,t)\\w(x,H,z,t)\end{bmatrix}=\begin{bmatrix}0\\0\\0\end{bmatrix}$$
$$\begin{bmatrix}u(x,y,0,t)\\v(x,y,0,t)\\w(x,y,0,t)\end{bmatrix}=\begin{bmatrix}u(x,y,W_{ch},t)\\v(x,y,W_{ch},t)\\w(x,y,W_{ch},t)\end{bmatrix}=\begin{bmatrix}0\\0\\0\end{bmatrix} \tag{5}$$

where H is the channel height and W_{ch} is the channel width. Thin-membrane moves in the y-direction only leading to zero tangential components of the velocity on the membrane:

$$\begin{aligned}u\left(x_f,y_f,z_f,t\right)&=0\\w\left(x_f,y_f,z_f,t\right)&=0\end{aligned} \tag{6}$$

In Eq. (6), x_f , y_f and z_f constitute the time-dependent position vector on the membrane; y_f is given by Eq. (1).

Y-velocity on the membrane is given by the time derivative of the displacement in Eq. (1) and (2):

$$v_f\left(x_f,t\right)=\omega B\cos\left(\omega t-kx_f\right)\min\left(t,\frac{1}{f}\right) \tag{7}$$

Inlet and outlet pressures are specified as zero in all simulations but for the ones used to obtain the the flow rate as a function of the pressure head for a typical pump:

$$\left[-P\mathbf{I}\right]\cdot\mathbf{n}\Big|_{x=0,y,z,t}=P_{in}=0 \tag{8}$$

$$\left[-P\mathbf{I}\right]\cdot\mathbf{n}\Big|_{x=L,y,z,t}=P_{out}=0 \tag{9}$$

For the flow at rest, all velocity components are specified as zero initially.

$$u\left(x,y,z,0\right)=v\left(x,y,z,0\right)=w(x,y,z,0)=0 \tag{10}$$

Displacement of the deforming mesh is calculated from the prescribed displacement given in Eq. (1) and (2), and expressed only for a limited domain surrounding the thin membrane:

$$\begin{aligned}&x_m=z_m=0,\\&y_m=\begin{cases}0, & x>\left|0.5\ell_f\right|\\ 4y_f\left(\dfrac{1}{4}-\left(\dfrac{y}{H}\right)^2\right), & \text{otherwise}\end{cases}\end{aligned} \tag{11}$$

The mesh displacement velocity, $\mathbf{u}_m$, in Eq. (3) is found directly from the prescribed mesh deformation:

$$\begin{aligned}&u_m=w_m=0\\&v_m=\frac{dy_m}{dt}=4\left(\frac{1}{4}-\left(\frac{y}{H}\right)^2\right)v_f\end{aligned} \tag{12}$$

Once $\mathbf{u}_m$ is obtained from Eq. (12), finite-element representation of Navier-Stokes and continuity equations, which are given by Eq. (3) and (4) are solved subject to boundary conditions in Eq. (5-9), and initial conditions in Eq. (10) with the commercial software COMSOL [17].

The instantaneous flow rate is computed by integrating the x-velocity over the inlet, or outlet of the channel:

$$Q\left(t\right)=\int_0^{W_{ch}}\int_{y=0}^{H}u\left(0,y,z,t\right)\mathbf{n}_{\{in,out\}}dydz \tag{14}$$

where $\mathbf{n}_{in}$ and $\mathbf{n}_{out}$ correspond to inlet and outlet surface normal vectors respectively. Time-averaged flow rate is computed from the integration of the instantaneous flow rate over at least two full cycles after the flow reaches to the steady-periodic state:

$$Q_{av}=\frac{f}{2}\int_{t_0}^{t_0+2/f}Q\left(t\right)dt \tag{15}$$

The y-component of the stress exerted on the fluid due to the membrane's motion on its surface is determined from the full stress tensor [18]:

$$\Sigma_y\left(x_m, y_m, z_m, t\right) = \begin{bmatrix} \mu\left(\dfrac{\partial u}{\partial y} + \dfrac{\partial v}{\partial x}\right) \\ \left(2\mu\dfrac{\partial v}{\partial y} - P\right) \\ \mu\left(\dfrac{\partial v}{\partial z} + \dfrac{\partial w}{\partial y}\right) \end{bmatrix} \cdot \mathbf{n} \qquad (16)$$

where **n** is the outward normal of the membrane's surface.

Instantaneous rate of work done on the fluid by the deforming membrane is the area integration of the product of the total *y*-stress and the *y*-velocity on the membrane, i.e.

$$\Pi(t) = \int_{A_f} \Sigma_y v_f \, dA_f \qquad (17)$$

Similarly to Eq. (15), time-averaged rate of work done by the membrane is calculated from:

$$\Pi_{av} = \frac{f}{2} \int_{t_0}^{t_0+2/f} \Pi(t)\, dt \qquad (18)$$

Hydraulic efficiency, η, of a typical micropump that consists of a thin-membrane, which deforms according to traveling-plane waves is calculated from the ratio of the fluid power, which is given by the multiplication of the total pressure head and the flow rate, and the rate of work done by the membrane as follows [19]:

$$\eta = \frac{\Delta P Q_{av}}{\Pi_{av}} \qquad (19)$$

RESULTS

Numerical results that are presented here are obtained for water flow in a pump whose dimensions are presented in Table 1. Nondimensional equations are used in the simulations. Characteristic scales used in the nondimensionalization are presented in Table 2. For each simulation, about 250000 linear equations are solved for at least 5 time units that correspond to 5 full cycles and between 500 to 1000 time steps. Simulation outputs converge to the steady-periodic state within the first cycle. Each simulation takes between 1 to 6 hours on a double dual-core 3.7 GHz 64-bit Xeon workstation with 16GB of RAM running on SUSE Linux 10.0 operating system depending on flow conditions characterized by the wave-amplitude, B_0, excitation frequency, f, and the ratio of the widths of the membrane and the channel, W_f/W_{ch}. Time-averaged quantities are obtained from integration over the last two cycles. Unless otherwise noted the base case used in the simulations corresponds to λ = 50 μm, B_0 = 5 μm, f = 112 Hz, and W_f/W_{ch} = 0.5.

In Fig. 2 and Fig. 3, pressure distribution on the center symmetry plane with deformed membrane structure and instantaneous streamlines are shown for the base case at t = 6. Pressure variations take place in the vicinity of the membrane away from the top and bottom walls of the channel parallel to the flow direction and away from the channel entrance and exit. Therefore it is reasonable to claim that there is a uniform flow at the channel entrance and exit owing to this localization of the pressure variations in the membrane's vicinity. Instantaneous streamlines are uniform near the inlet, exit and away from the membrane. Furthermore, having sides of the membrane exposed to the flow results in downstream vortex formations around and behind the membrane.

Figures 4, 5 and 6 demonstrate the velocity profiles on different sections of the half-channel as arrow plots for λ = 50 μm, B_0 = 5 μm, f = 112 Hz, and W_f/W_{ch} = 0.5 with W_{ch} = 200 μm at simulation time t = 6. Velocity field is steady in both inlet and outlet of the channel despite the large vortices formed by the free end of the membrane.

Name, symbol	Values/dimensions
W_{ch}	$W_f + 10^{-4}$ [m]
Channel Height, H	10^{-4} [m]
Channel Length, L	4×10^{-4} [m]
Membrane Length, ℓ_f	10^{-4} [m]
Wave Length, λ	$0.5\ell_f$ [m]
Dynamic Viscosity of water, μ	1.12×10^{-3} [Pa.s]
Density of water, ρ	999 [kg/m^3]

Table 1: Standard simulation parameters and their units

Characteristic scales	Representative values/dimensions
Length, ℓ_0	10^{-4} [m]
Time, t_0	$1/f$ [s]
Velocity, U_0	ℓ_0/t_0 [m/s]
Pressure and shear, p_0	ρU_0^2 [Pa]
Power, Π_0	$p_0 \ell_0^2 U_0$ [W]

Table 2: Characteristic scales and their values

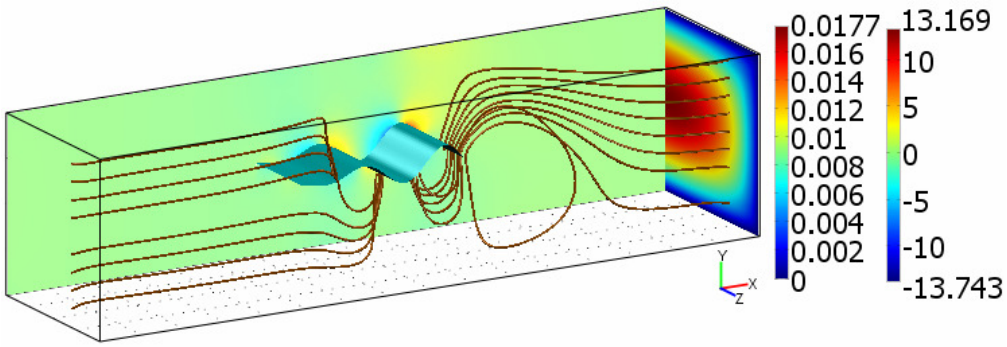

Figure 2: Snapshot of the streamlines from inlet and outlet of the channel both ending on bottom surface of the membrane, pressure distribution on the symmetry plane, and the exit velocity distribution at t = 6. First color bar stands for the nondimensional velocity profile on outlet half plane; second color bar stands for nondimensional pressure profile on the symmetry plane.

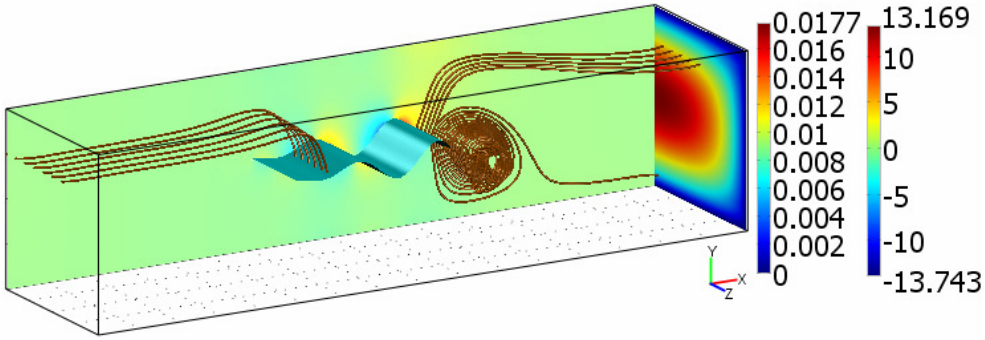

Figure 3: Snapshot of the streamlines from inlet and outlet of the channel both ending on top surface of the membrane with the circulation formed behind the membrane ending on outlet, pressure distribution on the symmetry plane, and the velocity distribution at the exit. First color bar stands for nondimensional velocity profile on outlet half plane; second color bar stands for nondimensional pressure profile on the symmetry plane.

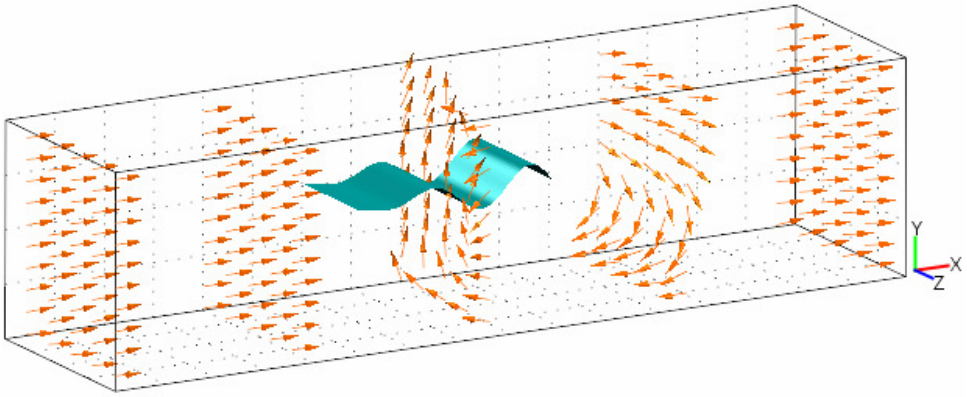

Figure 4: Normalized velocity vectors on yz-planes at x = -2, -1, 0, 1, 2.

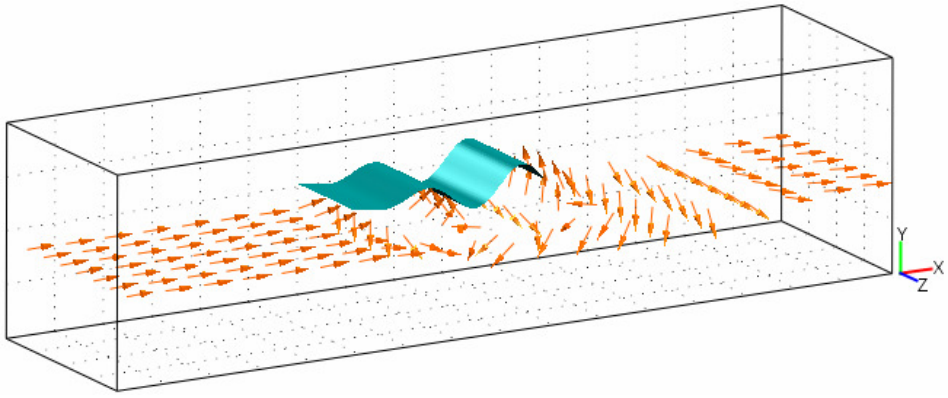

Figure 5: Normalized velocity vectors *xz*-plane at y = -0.1.

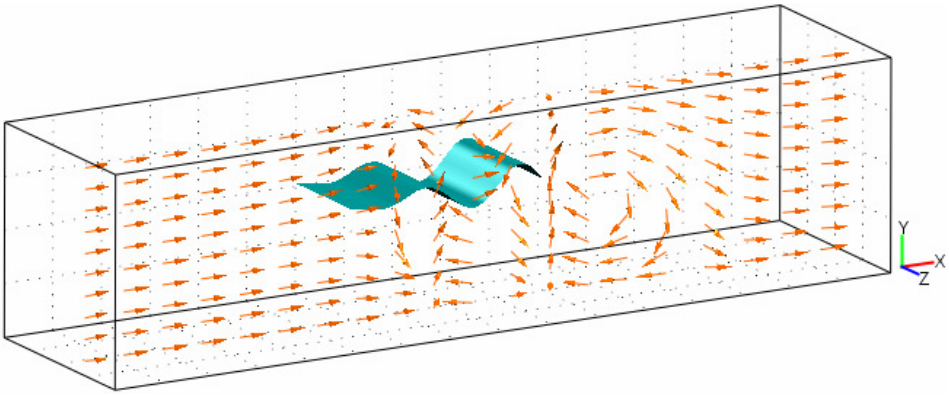

Figure 6: Normalized velocity vectors on *xy*-plane at z = 0.6.

Figure 7, demonstrates the relationship between the amplitude and the average flow rate for all the variables fixed at the base case except the amplitude. As amplitude increases the average flow rate increases quadratically with the amplitude which is in agreement with the asymptotical predictions [13,14] and our earlier 2D numerical results [15]. Slight deviation from quadratic relationship at large amplitudes is due to increased interaction of the three-dimensional flow with the channel walls. Further simulations are necessary to elucidate this deviation..

Figure 8 demonstrates the relationship between the wave-amplitude, B_0 and the time-averaged power consumption, Π_{av}, which is also quadratic with the amplitude, and in accordance with the asymptotic solutions given by Childress [9] and two-dimensional simulation results [15].

Figure 9 demonstrates the relationship between the average flow rate and the frequency for all the variables fixed at the base case except the frequency. In Fig. 9 a linear relationship between the frequency and the flow rate is observed as observed in 2D simulations also [15].

Figure 7: Amplitude vs. average flow rate for

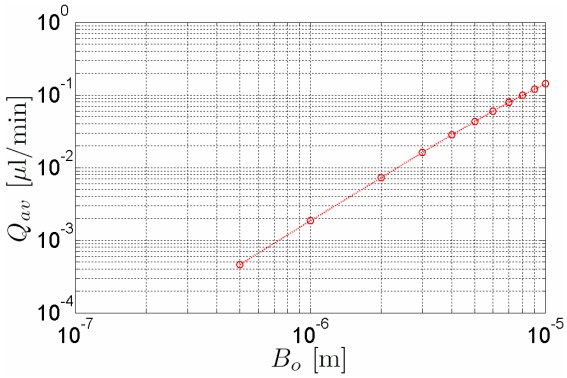

W_f/W_{ch} =0.5 and f = 112 Hz.

The average rate of work done on the fluid Π_{av} varies quadratically with the frequency as depicted in Fig. 10. The effect of the frequency, also, agrees well with the asymptotic results [13,14], where small amplitude choice was mathematically justified, and numerical results provided by our previous 2D simulations [15].

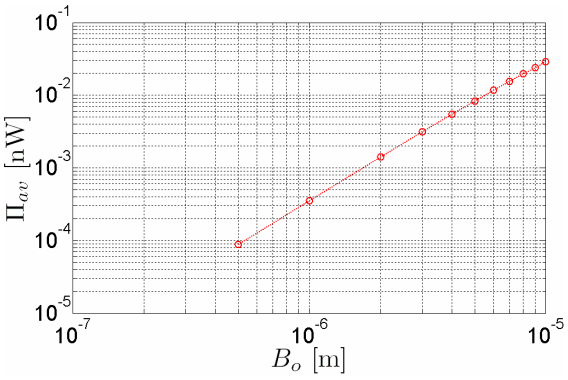

Figure 8: Amplitude vs. average power consumption for W_f/W_{ch} =0.5 and f = 112 Hz.

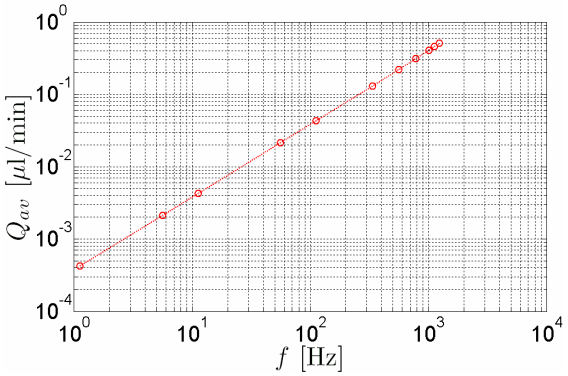

Figure 9: Frequency vs. average flow rate for $\lambda = 0.5\ell_f = 0.5H = 0.5W_f$ = 50 μm, W_f/W_{ch} =0.5 and $B_o = H/20$ = 5 μm.

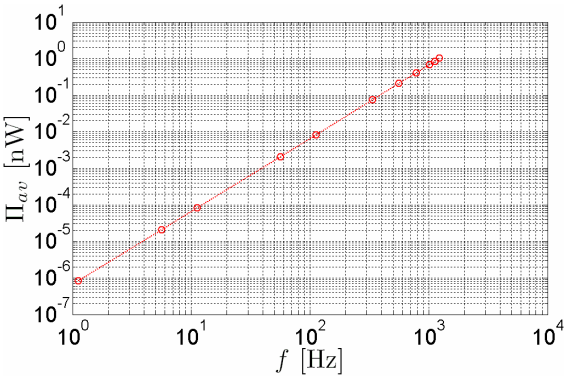

Figure 10: Frequency vs. average power consumption for W_f/W_{ch} = 0.5 and B_o = 5 μm.

Figures 11 and 12, display the effect of the ratio of the membrane's width to the channel width on the average flow rate and the rate of work done on the fluid. In simulations that correspond to data points on the graph width ratio is adjusted by means of adjusting the membrane's width and fixing the other variables at the base case. As the width of the channel approaches to the width of the membrane, i.e. $W_f/W_{ch} \to 1$, not only the flow rate (Fig. 11) but also the average power increases rapidly, hinting that the gap between the membrane and the channel's side walls play a very important role in addition to increasing membrane area. In fact, when the ratio goes to zero, i.e. $W_f/W_{ch} \to 0$, both the power and the flow rate increases almost linearly.

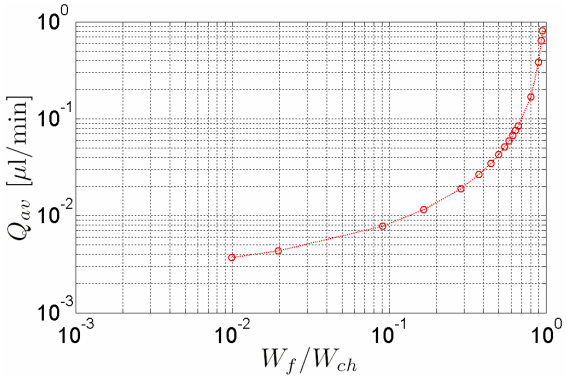

Figure 11: W_f/W_{ch} vs. average flow rate for B_o = 5 μm and f = 112 Hz.

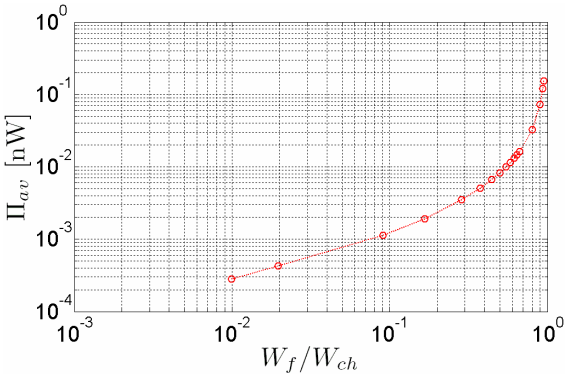

Figure 12: W_f/W_{ch} vs. average power consumption for B_o = 5 μm and f = 112 Hz.

The average flow velocity, which is given by Q_{av}/A_{ch}, is plotted against the width ratio in Fig. 13. Clearly, as the ratio increases, i.e. the membrane width increases, the membrane becomes more effective in propulsion. For large width ratios, $W_f/W_{ch} >$ 0.5, as the width ratio decreases momentum flux into the z-direction drains the available mechanical energy and reduces the net propulsion. On the other hand, for small width ratios, the average velocity tends to approach a limit, which, presumably, corresponds to the average velocity of the swimmer in an infinite medium.

Area averaged power consumption, which is given by Π_{av}/A_f, is plotted against the width ratio in Fig. 14. Even though total power consumption increases, power consumption per unit area drops al-

most linearly for small width ratios, which may be due to decreasing flow in the z-direction. For large width ratios, area-averaged rate-of-work done on the fluid does not vary significantly.

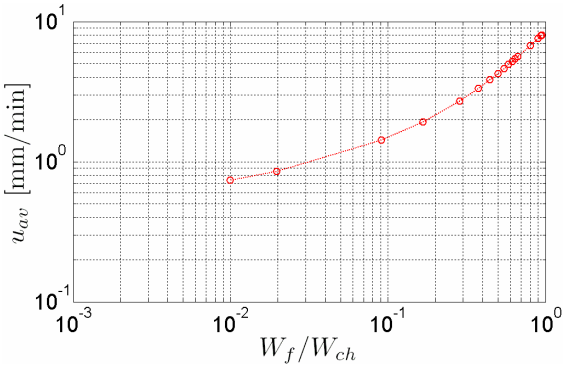

Figure 13: W_f/W_{ch} vs. average velocity for B_o = 5 μm and f = 112 Hz.

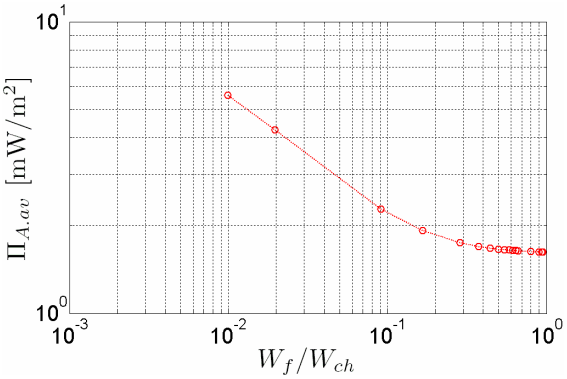

Figure 14: W_f/W_{ch} vs. power consumption per unit area for B_o = 5 μm and f = 112 Hz.

Pressure head and efficiency versus the flow rate are shown in Fig. 15 for the micropump that operates at the base case, for which B_0 = 5 μm, W_f/W_{ch} = 0.5 with and f = 112 Hz. For simulations that correspon to the date points in the figure, outlet pressure is kept at zero and the inlet pressure is varied. Calculated flow rates for the prescribed pressure difference between the exit and the inlet, $\Delta P = P_{out} - P_{in}$, are shown in Fig. 15. Furthermore, the efficiency of the micropump is calculated from Eq. (19) and plotted as a function of the average-flow rate on the right-axis of the plot in Fig. 15. Similarly to an ideal pump, the pressure head vs. the flow rate is linear, and the efficiency is parabolic. The maximum flow rate for zero pressure head and the maximum pressure head for zero flow rate are about 0.04 μl/min and 40 mPa respectively. Moreover, the maximum efficiency takes place at the half of the maximum flow rate, i.e. Q_{av} = 0.02 μl/min, and is 0.085%. Note that, in general, micro fluidic devices have small efficiencies because of the dominance of the viscous effects [5].

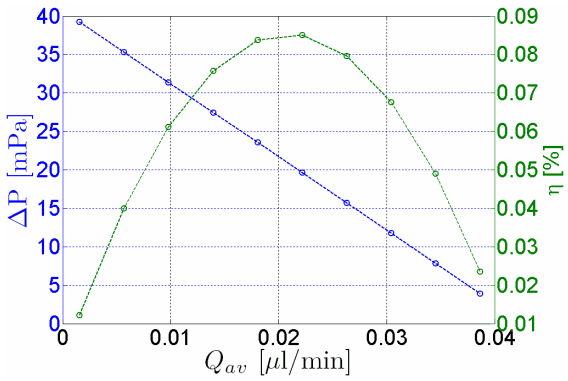

Figure 15: Pressure head (blue circles, left axis) and efficiency (green circles, right axis) of the micropump as a function of the flow rate. Each data point corresponds to a numerical simulation for which pressure boundary conditions are specified according to the corresponding pressure head.

CONCLUSION

A biologically inspired micropump actuation mechanism is reported here. The effects of some of the performance variables such as the wave amplitude, excitation frequency and width ratio between membrane and channel are demonstrated by means of three-dimensional time-dependent simulations of the flow. Flow induced by traveling-plane-wave deformations on the thin-membrane that has finite dimensions and is placed inside a channel is modeled by incompressible Navier-Stokes equations on a deforming mesh due to moving boundaries. Deformation of the mesh is prescribed and an arbitrary Lagrangian Eulerian method is used to ensure the physical solution.

Based on our numerical results, the flow rate increases linearly with the excitation frequency and quadratically with the amplitude. Similarly, the dependence of the rate-of-work done on the fluid is quadratic with both the frequency and the amplitude. The average velocity of the flow increases almost linearly with the increasing width of the membrane. However, the area-averaged power tends to converge to a limit as the width ratio increases. Therefore, from the geometric design point-of-view, it is recommended to limit the space between the membrane and the channel's side walls for better efficiency and higher flow rates.

Finally, the performance of a typical micropump that uses traveling-plane-wave deformations on a thin membrane inside a channel for flow and pressure head is obtained and reported. The micropump has similar characteristics compared to its counterparts using other mechanisms.

ACKNOWLEDGMENTS

We kindly acknowledge the partial support for this work from the Sabanci University Internal Grant Program (contract number IACF06-00418).

REFERENCES

[1] Purcell, E.M., 1977, "Life at Low Reynolds Number," American Journal of Physics, 45(1), pp. 3-11.

[2] Brennen, C., Winet, H., 1977, "Fluid Mechanics of Propulsion by Cilia and Flagella," Ann. Rev. Fluid Mech., 9, pp. 339-98.

[3] Gray, J., Hancock, G.J., 1955, "Propulsion of Sea-Urchin Spermatozoa," J. Exp. Biol., 32, pp. 802-814.

[4] Lowe, C.P., 2003, "Dynamics of Filaments: Modeling the Dynamics of Driven Microfilaments," Phil. Trans. R. Soc. Lond., B(358), pp. 1543-1550.

[5] Laser, D.J., Santiago, J.G., 2004, "A Review of Micropumps," J. Micromech. Microeng., 14, pp. R35-R64.

[6] Edd, J., Payen, S., Rubinsky, B., Stoller, M.L., Sitti, M., 2003, "Biomimetic Propulsion for a Swimming Surgical Micro-Robot," IEEE/RSJ Intelligent Robotics and Systems Conference, Las Vegas, USA.

[7] Dreyfus, R., Baudry, J., Roper, M.L., Fermigier, M., Stoner, H.A., Bibette, J., 2005, "Microscopic Artificial Swimmers," Nature, 437, pp. 862-865.

[8] Nguyen, N.T., White, R.M., 1999, "Design and Optimization of an Ultrasonic Flexural Plate Wave Micropump Using Numerical Simulation," Sensors and Actuators, 77, pp. 229-236.

[9] Childress, S., 1981, Mechanics of Swimming and Flying, Cambridge Studies in Mathematical Biology, Cambridge University Press, New York, Chap. 3.

[10] Piefort, V., 2001, "Finite Element Modelling of Piezoelectric Active Structures. PhD Thesis submitted to Faculty of Applied Sciences," Université Libre De Bruxelles.

[11] Piefort, V., Henrioulle, K., 2000, "Modelling of Smart Structures with Colocated Piezoelectric Actuator/sensor Pairs: Influence of the In-plane Components," Identification, Control and Optimization of Engineering Structures, Civil-Comp Press, Edinburgh, UK.

[12] Tabak, A.F., 2007, "Micropropulsion System Design," MS Thesis to be submitted to Faculty of Engineering and Natural Sciences, Sabanci University, (in preparation).

[13] Sir Taylor, G., 1951, "Analysis of the Swimming of Microscopic Organisms," Proc. Roy. Soc., A(209), pp. 447-61.

[14] Katz, D.F., 1974, "On the Propulsion of Micro-organisms Near Solid Boundaries.," J. Fluid Mech., 64(1), pp. 33-49.

[15] Tabak, A.F., Yeşilyurt, S., 2007, "Numerical Simulations and Analysis of a Micropump Actuated by Traveling Plane Waves," SPIE-Photonics West, MOEMS-MEMS, San Jose.

[16] Duarte, F., Gormaz, R., Natesan, S., 2004, "Arbitrary Lagrangian-Eulerian Method for Navier-Stokes Equations with Moving Boundaries," Comput. Methods Appl. Mech. Engrg., 193, pp. 4819-4836.

[17] COMSOL AB, 2005, Comsol Multiphysics Modelling Guide.

[18] Landau, L.D., Lifshitz, E.M., 2005, Fluid Mechanics 2nd ed., Course of Theoretical Physics v.6, Elsevier Butterworth-Heinemann, Oxford, Chap. 2.

[19] Munson, B.R., Young, D.F., Okiishi, T.H., 2006, Fundamentals of Fluid Mechanics John Wiley & Sons, Inc., USA, Chap. 12.